

Article

The Effect of pH and Viscosity on Magnetophoretic Separation of Iron Oxide Nanoparticles

Leonie Wittmann , Chiara Turrina  and Sebastian P. Schwaminger * 

Bioseparation Engineering Group, Department of Mechanical Engineering, Technical University of Munich, Boltzmanstr. 15, 85748 Garching bei München, Germany; l.wittmann@tum.de (L.W.); c.turrina@tum.de (C.T.)
* Correspondence: s.schwaminger@tum.de

Abstract: Magnetic nanoparticles (MNPs) are used for magnetophoresis-based separation processes in various biomedical and engineering applications. Essential requirements are the colloidal stability of the MNPs and the ability to be separated even in low magnetic field gradients. Bare iron oxide nanoparticles (BIONs) with a diameter of 9.2 nm are synthesized via coprecipitation, exhibiting a high saturation magnetization of $70.84 \text{ Am}^2 \text{ kg}^{-1}$ and no remanence. In our study, zeta potential, dynamic light scattering (DLS), and sedimentation analysis show that the aggregation behavior of BIONs is influenced by pH and viscosity. Small aggregate clusters are formed with either low or high pH values or increased viscosity. Regarding magnetophoresis-based separation, a higher viscosity leads to lower magnetophoretic velocities, similar to how small aggregates do. Additionally, cooperative magnetophoresis, the joint motion of strongly interacting particles, affects the separation of the BIONs, too. Our study emphasizes the effect of pH and viscosity on the physicochemical characteristics of MNPs, resulting in different aggregation behavior. Particularly, for high viscous working media in downstream processing and medicine, respectively, the viscosity should be taken into account, as it will affect particle migration.



Citation: Wittmann, L.; Turrina, C.; Schwaminger, S.P. The Effect of pH and Viscosity on Magnetophoretic Separation of Iron Oxide Nanoparticles. *Magnetochemistry* **2021**, *7*, 80. <https://doi.org/10.3390/magnetochemistry7060080>

Academic Editor: Marie Frenea-Robin

Received: 29 April 2021

Accepted: 30 May 2021

Published: 3 June 2021

Publisher's Note: MDPI stays neutral with regard to jurisdictional claims in published maps and institutional affiliations.



Copyright: © 2021 by the authors. Licensee MDPI, Basel, Switzerland. This article is an open access article distributed under the terms and conditions of the Creative Commons Attribution (CC BY) license (<https://creativecommons.org/licenses/by/4.0/>).

Keywords: magnetophoresis; magnetic separation process; iron oxide nanoparticles; aggregation; pH; viscosity; sedimentation analyzer; zeta potential; hydrodynamic diameter

1. Introduction

Magnetic nanoparticles (MNPs) have become an important nanomaterial in biotechnology, in chemistry, and in medicine [1–6]. They entail characteristics such as biocompatibility, high binding capacities, and cost-efficient production via coprecipitation. Moreover, their superparamagnetic properties are advantageous during the separation process, as the MNPs show no remanence at room temperature. However, when applying a magnetic field, they possess a high magnetic susceptibility and can be easily separated [7,8]. For biological samples, it is challenging to separate a target entity from a complex mixture with different components. Here, magnetophoresis-based processes provide a simple and efficient method, where the desired entity (magnetic or magnetically labeled with MNPs) is isolated by applying an external magnetic field [9–11]. For the method of High Gradient Magnetic Separation (HGMS), a suspension containing the magnetic material is pumped through a separation chamber, and it is trapped by a magnetically susceptible matrix due to high magnetic field gradients (10^2 – 10^4 T m^{-1}) [9,11,12]. In contrast, low magnetic field gradients ($<100 \text{ T m}^{-1}$) are used for Low Gradient Magnetic Separation (LGMS), where a magnet is placed outside the particle suspension without contacting the particles [13]. Both modes of operation can be realized with either a permanent magnet or an electromagnet. However, the latter brings up several challenges. The installation costs are higher than a permanent magnet, and cooling might be necessary to counteract the Joule heating. Thus, water usage is required besides energy consumption [14]. Therefore, a permanent magnet might be preferred in the biomedical field. Moreover, in microfluidics, the implementation

of a permanent magnet with a high magnetic field gradient is more advantageous, as Alnaimat et al. summarize [15].

For LGMS or HGMS applications, such as in microfluidics [16] or in medicine [17–22], it is important to have a defined and stable particle size. Hence, MNPs need to meet the following requirements. On the one hand, they should be colloidal stable and not form aggregates so that they remain their defined size during fractionation or separation [5]. Particularly, for medical purposes, such as hyperthermia treatment or magnetic resonance imaging, the particle diameter should be smaller than 100 nm without forming large aggregates [17,19,23,24]. On the other hand, it should be possible to isolate the colloidal stable MNPs with the respective magnetic field gradient [25].

Regarding downstream processing, the handled liquids, e.g., cell lysates or hydrolysates coming out of fermentation, pose another challenge. Viscosity becomes an essential factor, influencing the separation performance [26–28]. Furthermore, in medical applications, the medium blood exhibits a higher viscosity, being fivefold higher than the one of water [29]. In addition to the higher viscosity, serum proteins or other blood components might influence the aggregation behavior [20,21]. However, the so-called biocorona, which is determined by the liquid components such as biomolecules, bacterial debris, proteins, or lipids, could also prevent the aggregation of MNPs [30]. Socoliuc et al. recently emphasized the importance of characterizing the aggregation behavior of MNPs in the respective medium, e.g., cell culture media, and not only in water [18]. Besides the intrinsic characteristics of the working liquid, an increase in viscosity could be advantageous for the microfluidic processing of magnetic particles [31]. In order to avoid sedimentation effects during the process, Solsona et al. developed a microfluidic chip for the magnetophoretic sorting of single-catalyst particles composed of iron [31]. Hence, working with different viscosities might facilitate process handling, or a specific medium might give another viscosity. We would like to point out that besides other parameters, e.g., pH, the viscosity might influence the particle aggregation behavior as well.

Concerning an LGMS process, the control of aggregation is important, as it has been shown that, despite low magnetic field gradients, the particles can be separated, mainly due to cooperative magnetophoresis [32–34]. By extending the DLVO theory with the magnetic interaction, this phenomenon can be explained [35]. Here, particles form aggregates because of the magnetic field gradient, as their magnetic dipoles align, and the cooperative effect speeds up the magnetophoretic separation. According to Faraudo et al., these aggregates are reversible for high zeta potentials. Electrostatic repulsion and magnetic attraction form a secondary minimum besides the primary one, separated by a potential barrier [35]. The magnetic Bjerrum length poses a parameter, which enables the evaluation of aggregation throughout a magnetophoretic process. It describes the distance of two parallel dipoles, where the magnetic force equals the thermal energy. Due to this parameter, it can be estimated if the magnetic dipoles are interacting with each other or not.

$$\lambda_B = \frac{\mu_0 \cdot m^2}{2 \cdot \pi \cdot k_B \cdot T}^{\frac{1}{3}} \quad (1)$$

The Bjerrum length is dependent on the permeability of free space $\mu_0 = 4\pi \times 10^{-7} \text{ H m}^{-1}$, the Boltzmann's constant $k_B = 1.381 \times 10^{-23} \text{ J K}^{-1}$, the temperature T , and the magnetic dipole, which is written as

$$m = M_S \cdot \rho_p \cdot \frac{4}{3} \cdot \pi \cdot r^3, \quad (2)$$

where the saturation magnetization per unit mass of colloid is M_S , the particle density is ρ_p , and the particle radius is r .

This study emphasizes the importance of understanding the aggregation behavior of bare iron oxide nanoparticles (BIONs) in different viscosities. The influence on a separation process in a low magnetic field gradient is investigated by the magnetophoretic sedimentation velocity with a sedimentation analyzer. The following hypotheses are proposed:

1. The aggregation behavior of BIONs in the gravity field is dependent on pH and viscosity, respectively. Therefore, the colloidal stability can be selectively controlled.
2. During magnetophoresis, these effects directly influence the separation process. The aggregate size, as well as viscosity, result in different magnetophoretic velocities.

Four different pH values between 4 and 9, which clearly show the pH's influence on aggregate size and therefore on magnetophoretic sedimentation velocity, are chosen. The viscosity of water ($\eta = 0.888$ mPa s) is compared with the 2.5-fold viscosity. A higher viscosity can be beneficial for magnetophoretic sorting processes, as field-induced aggregation and convection only play a minor role at elevated viscosities [31,33]. The higher viscosity is obtained by adding sucrose ($\eta = 2.227$ mPa s).

2. Results and Discussion

2.1. Particle Characterization

BIONs are synthesized via coprecipitation. They exhibit a high saturation magnetization of $70.84 \text{ Am}^2 \text{ kg}^{-1}$ (Figure 1a), no remanence and no hysteresis at 0 Oe [36–38]. The chemical composition and the crystalline spinel structure were previously described by Schwaminger et al. [39]. With Transmission Electron Microscopy (TEM) (Figure 1b), the optical diameter of the BIONs is examined, resulting in an average single particle diameter of 9.92 nm, which is similar to previous measurements of BIONs [38–40].

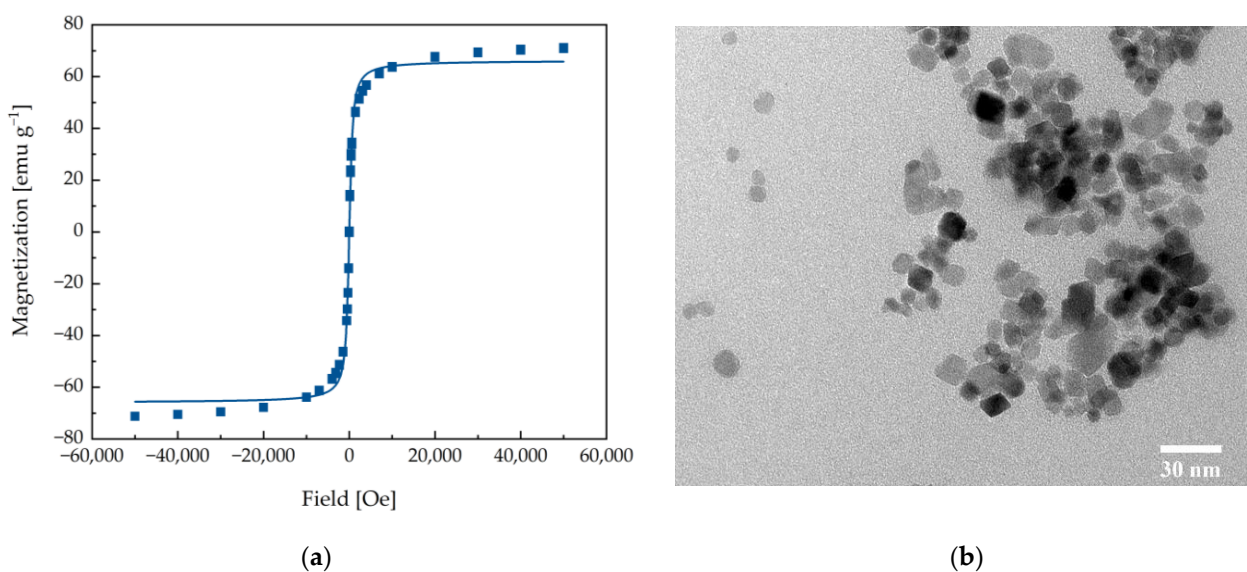


Figure 1. (a) Superconducting quantum interference (SQUID) measurement for the bare iron oxide nanoparticles (BIONs) at 300 K with a LangevinMod fit. (b) Transmission Electron Microscopy (TEM) image of the BIONs.

2.2. Influencing the Colloidal Stability of the BIONs due to Viscosity and pH

Zeta potential is the electrostatic potential at the particle's slipping plane, which presents the interface between the moving fluid and the fluid attached to the particle surface. Therefore, the zeta potential is used as a relative measurand for the surface potential and, thus, for the magnitude of a particle's charge. Due to the extent of electric repulsion between the particles in the solution, the colloidal stability can be evaluated. The repulsion energy is thereby dependent on the particles' radius and the extent of shielding, which is affected by the ionic strength of the solvent [41]. Figure 2 illustrates the course

of zeta potential versus pH and presents the amphiphilic character of the BIONs' surface. At very low and high pH, it ranges between 20 and 35 mV or -20 and -35 mV, meaning the BIONs' net charge is positive or negative, respectively. Thus, the particles' repulsion is high, and they are colloidally stable, leading to less aggregation. The hydrodynamic diameter measurement goes in line with this assumption, as it shows low diameters for low and high pH values. While the isoelectric point (IEP), where the potential is 0, is 6.69 for the low viscous solution ($\eta = 0.888$ mPa s) (Figure 2a), it is 6.07 for the high viscous solution ($\eta = 2.227$ mPa s) (Figure 2b) [42]. Here, the particles form aggregates up to 3000 nm in both liquids because of their low superficial charge. Comparing the particle distributions of both solutions, the one with the low viscosity (Figure 2a) exhibits a wide distribution over pH. In contrast, for the other one (Figure 2b), large aggregates can only be observed at pH 5 and 6. Thus, in the higher viscous solution, the colloidal stability of the BIONs is given over a broader pH range from pH 2 to 4 and pH 7 to 10. In addition, the polydispersity index (PDI) of the measured samples (Figure S1) confirms these results, as it is between 0.18 ± 0.09 and 0.24 ± 0.04 for the high viscous solution, whereas it is between 0.22 ± 0.03 and 0.54 ± 0.20 for the low viscous solution. Compared to the literature, a PDI below 0.7 is considered as nearly monodisperse [43]. For pH 2, 3, 9, and 10, the PDI for both solutions is similar; however, for the low viscous samples, the PDI at pH 5, 6, 7, and 8 is higher. This indicates that the BIONs around the IEP possess a higher heterogeneity in aggregate size. Additionally, this effect can be seen in the intensity distributions of all samples in Figures S2 and S3. For the water solution, heterogeneous aggregates are detected between pH 4 and 8, while the particle distributions for the higher viscosity are uniform. Particularly, for low pH values, the particles might react with the acid and therefore possess a higher stability.

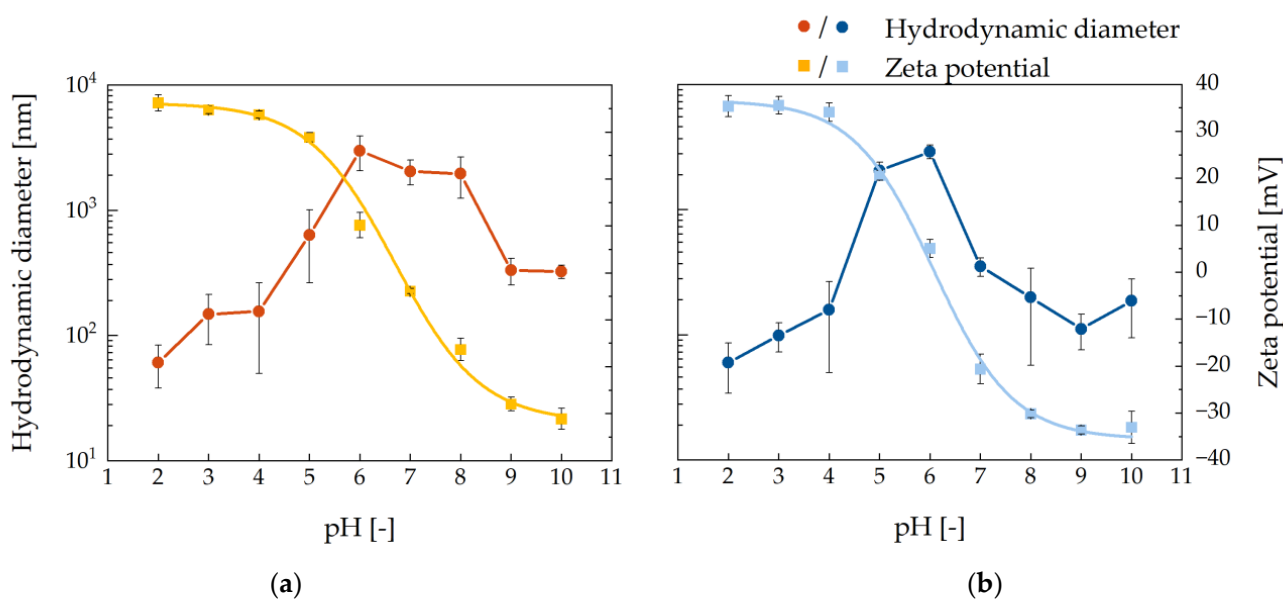


Figure 2. Hydrodynamic diameter and zeta potential measurements of BION suspension in pH 2 to 10 (a) in deionized water ($\eta = 0.888$ mPa s) (b) and sucrose solution ($\eta = 2.227$ mPa s).

The analysis of BIONs in other sugar solutions, such as fructose and glucose, at pH 7 resulted in similar particle distributions as sucrose (Figure S4). In the literature, the effect on the colloidal stability of particles due to higher viscosity by sugars, such as sucrose, is confirmed. Previously, Szalai et al. synthesized ex situ coated magnetite nanoparticles with gelatin and sucrose. They reported higher colloidal stability of their particles when adding sucrose [44]. Sun et al. propose that the multiple hydroxyl groups, as they are present in sucrose, can adsorb or chelate onto the magnetite surface, resulting in steric hindrance, as it is known to conventional surfactants [45,46]. Benítez et al. describe another effect of sugars,

where they claim that sucrose might influence particles' colloidal stability because of the hydration capacity. They extend the DLVO theory by the hydration repulsive energy, which occurs as water molecules around the particle surface restrict them in their motion, known as hydration pressure [47,48]. We assume that stabilization due to the higher viscosity with sucrose is reached because of a synergy of the mentioned effects.

2.3. Dependence of the Magnetophoretic Velocity on Aggregate Size and Viscosity

The effect of pH and viscosity on the aggregation behavior of our BIONs indicates that it is essential to evaluate the influence of different aggregate sizes regarding a magnetophoresis-based separation process. The Space-and-Time-resolved Extinction Profiles (STEP) technology is based on the sedimentation of particles due to magnetophoresis. It describes the particles' movement towards the magnetic field direction if the buoyancy and friction force is overcome (Figure 3).

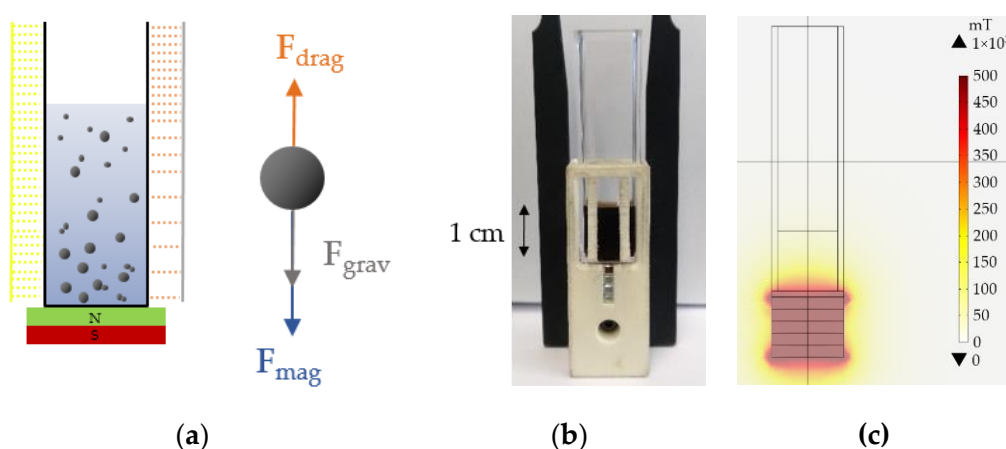


Figure 3. (a) Schematic illustration of the sedimentation analyzer (LUMiReader) with the involved forces (magnetic force F_{mag} , the gravitational force F_{grav} , and the drag force F_{drag}). (b) Experimental set-up. The cuvette filled with sample fluid is placed on a magnet, and parallel light with a wavelength of 870 nm transmits the sample. A light sensor records transmission profiles, and the magnetophoretic velocity of the particles is calculated. The magnetic flux density in the direction of the particle movement is 40 mT at the sample top and 350 mT at the sample bottom. (c) Calculated magnetic flux density along the y -axis. Calculations were performed with COMSOL Multiphysics 5.6.

Figure 4 presents the magnetophoretic velocity derived from STEPs over pH 4, 6, 7, and 9 at $\eta = 0.888$ and $\eta = 2.227$ mPa s. For pH 4 and 9, the magnetophoretic velocity is noticeably lower than for pH 6 and 7, which goes in line with the measured particle size distributions via dynamic light scattering (DLS) measurement (Figure 5). The latter pH values show around one power of ten higher diameters than pH 4 and 9 because the surface of the BIONs is charged positively or negatively, respectively. Hence, the attractive forces major the repulsive ones so that the particles do not resist aggregation. The same pattern can be observed for the high viscous samples. Here, at pH 6, which is almost the IEP of the BIONs, aggregates with a hydrodynamic diameter of 2764 ± 446 nm show a higher magnetophoretic velocity in contrast to other pH values where the hydrodynamic diameter is smaller (Figure 5b). Here, for pH 4, 7, and 9, a second mode with larger aggregates is detected, which is not visible in the intensity distributions (Figure S2). Even if the amount of these larger aggregates is lower compared to the first mode, they might influence the measured magnetophoretic velocity. The velocity differences are lower compared to the less viscous samples. Following Equation (7), the particle radius is directly proportional to the magnetophoretic force during the sedimentation process. Therefore, the measured velocities are in line with the theoretical assumptions.

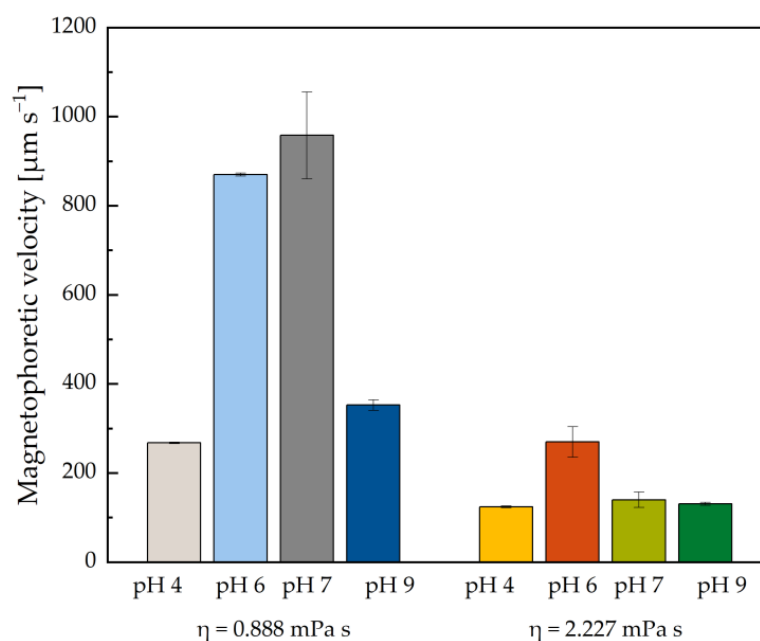


Figure 4. Magnetophoretic velocity over pH 4, 6, 7, and 9 of BION suspension in deionized water ($\eta = 0.888 \text{ mPa s}$) and sucrose solution ($\eta = 2.227 \text{ mPa s}$) with a corresponding mean diameter of DLS measurement.

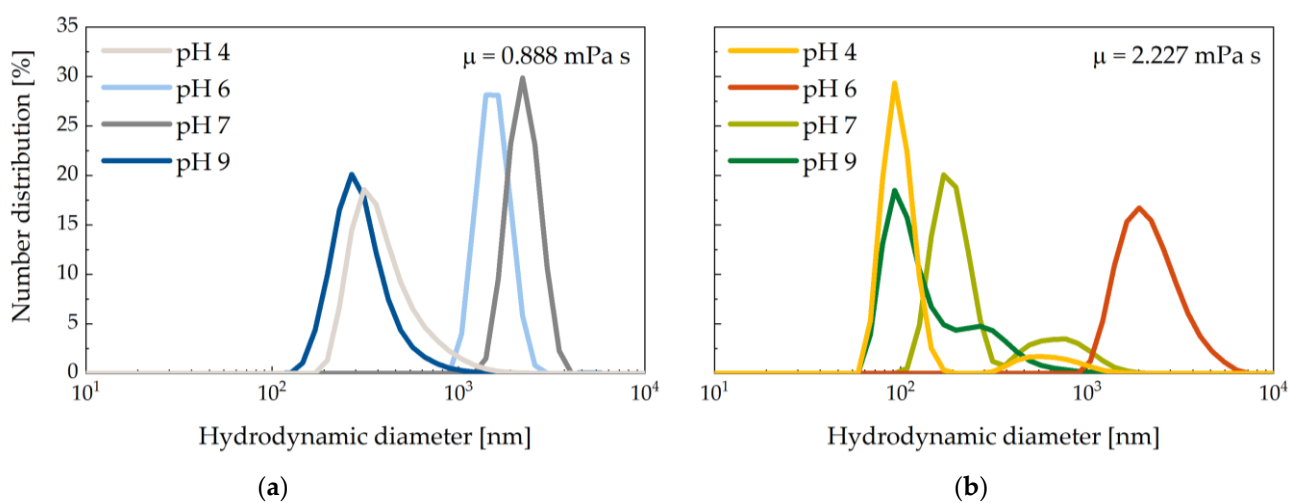


Figure 5. Particle size distribution at pH 4, 6, 7, and 9 of BION suspension (a) in deionized water ($\eta = 0.888 \text{ mPa s}$) (b) and sucrose solution ($\eta = 2.227 \text{ mPa s}$).

Besides the aggregate size, viscosity is another parameter that influences the separation process. The magnetophoretic velocities of all measured pH values are lower for the higher viscosity ($\eta = 2.227 \text{ mPa s}$) compared to the lower one ($\eta = 0.888 \text{ mPa s}$), as the viscosity is indirectly proportional to the velocity, as written in Equation (10). Due to the higher viscosity, the drag force increases and slows down the particle motion along the magnetic field gradient. The gravitational force does not influence this effect, as values for the sedimentation velocity show very low values for both viscosities (Table 1). Here, the sedimentation velocity is similar when having the same size of aggregates at different pH values only in a gravitational field.

Taking these findings together, the viscosity influences the colloidal stability of the particles and the magnetophoresis process itself. These effects should be taken into account when working with high viscous liquids, such as cell lysates or blood, in order to obtain a distinct separation process.

Table 1. Measurement of the sedimentation velocity and the corresponding hydrodynamic diameter of the samples in the sedimentation analyzer.

pH	$\eta = 0.888 \text{ mPa s}$		$\eta = 2.227 \text{ mPa s}$	
	Sedimentation Velocity ($\mu\text{m s}^{-1}$)	Hydrodynamic Diameter (nm)	Sedimentation Velocity ($\mu\text{m s}^{-1}$)	Hydrodynamic Diameter (nm)
4	1.57 ± 0.09	156 ± 106	0.88 ± 0.70	158 ± 108
6	3.82 ± 0.85	2986 ± 920	2.30 ± 0.01	2764 ± 446
7	3.69 ± 0.14	2047 ± 461	0.33 ± 0.28	351 ± 58
9	1.43 ± 0.37	331 ± 79	0.31 ± 0.06	111 ± 35

Regarding a LGMS process, the particle size poses an essential factor in the kinetics of the separation and the resulting process efficiency. As mentioned above, mainly the cooperative effect of magnetic aggregation speeds up the magnetophoretic motion of the particles [49]. Here, the Bjerrum length can be used in order to evaluate the formation of aggregates in a magnetic field [9,50]. Therefore, we calculate the ratio of the Bjerrum length λ_B and the particle diameter d (Figure 6). As seen in Figure 6, particles do not form aggregates in a magnetic field if $\lambda_B d^{-1} < 1$ with a saturation magnetization of $70.84 \text{ Am}^2 \text{ kg}^{-1}$ [49]. For our BIONs with a particle diameter of 9.92 nm , the ratio is 1.12 , which implies magnetic aggregate formation. This value, measured by TEM, is close to one; however, this is the minimal limit, as the particle diameter in suspension is $>100 \text{ nm}$, depending on the buffer conditions. Hence, the magnetophoretic velocity might be additionally influenced by this effect, but from a practical process view, cooperative magnetophoresis might be beneficial to implement such an LGMS process because the separation efficiency increases.

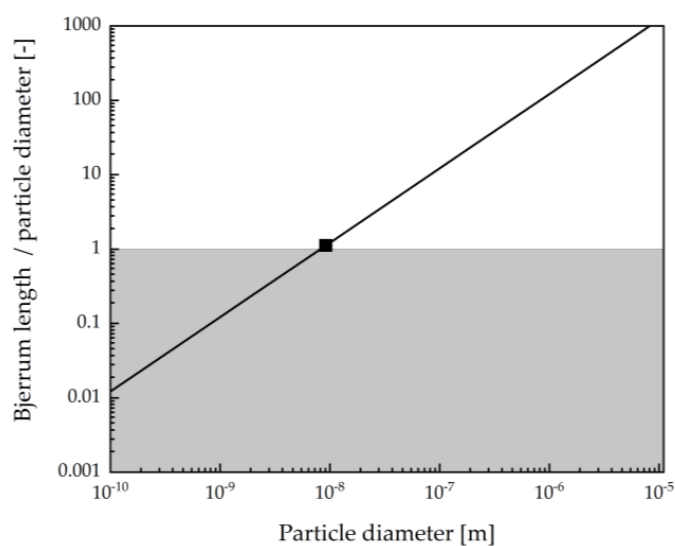


Figure 6. Log–log plot of the ratio of the Bjerrum length and the particle diameter over the particle diameter. The shaded region corresponds to particle diameters where no aggregation due to a magnetic field occurs, and the solid line describes the Bjerrum length for particles with the same magnetization. The symbol represents our particle size and indicates that magnetic aggregation takes place (transparent region).

Besides the cooperative magnetophoresis, Leong et al. recently discussed the effect of convective magnetophoresis [33,41]. They introduce the dimensionless Grashof number Gr_m (Equation (3)), which is dependent on the magnetic field gradient ∇B , the volumetric

magnetization M , the particle concentration difference between the bulk solution, the collection plane $c_s - c_\infty$ and the length of the analyzed system L_c .

$$Gr_m = \frac{\rho \cdot \nabla B \cdot \left(\frac{\partial M}{\partial c} \right)_H \cdot (c_s - c_\infty) \cdot L_c^3}{\eta^2} \quad (3)$$

It describes the convection induced by an external magnetic field, which happens due to the rapid acceleration of the particles. Leong et al. state that the Grashof number is mostly dependent on the concentration, resulting in a higher magnetophoretic velocity for higher particle concentrations. However, in our study, all parameters are kept constant besides the viscosity. Its square is indirectly proportional to the dimensionless number, so one can say that an increase in viscosity lowers the convection and therefore, the magnetophoretic velocity as well.

In addition to both discussed effects, the cooperative and the convective magnetophoresis, the diffusion, described by the Stokes–Einstein Equation, is influenced by viscosity as shown in Equation (4) [51]:

$$D_o = \frac{k_B \cdot T}{6 \cdot \pi \cdot r \cdot \eta} \quad (4)$$

According to Equation (4), the diffusion coefficient is decreasing with a higher viscosity and thus, Brownian motion is lower as well. Hence, it evolves that viscosity noticeably influences various parameters during a magnetophoresis-based process and should be always considered.

To sum up, the colloidal stability of BIONs is controllable due to a change in pH value, but also a higher viscosity leads to stabilization. The former is based on electrostatic stabilization effects, whereas the various latter effects, such as a steric hindrance and/or hydration repulsion due to sucrose, might be involved. The different aggregate sizes and the viscosity influences the magnetophoresis process (Equations (5)–(10)). Particularly, for a separation process with high viscous liquids, the efficiency is lower [26]. Moreover, depending on the aggregate size, MNP–MNP interactions, as cooperative or convective magnetophoresis and Brownian motion, have to be considered, as these effects influence magnetophoretic processes, e.g., a microfluidic fractionation.

3. Materials and Methods

Coprecipitation of $Fe^{2+}/3+$ ions was used to synthesize the BIONs [38]. For this, 28.9 g of sodium hydroxide (722 mmol, 4.10 equivalents (eq.), Carl Roth GmbH + Co. KG, Karlsruhe, Germany) was dissolved in 400 mL of degassed water under a nitrogen atmosphere. A solution, containing 86.6 g of $FeCl_3 \cdot 6H_2O$ (320 mmol, 1.82 eq., Sigma Aldrich Merck KGaA, Darmstadt, Germany) and 35.0 g of $FeCl_2 \cdot 4H_2O$ (176 mmol, 1.0 eq., Sigma Aldrich Merck KGaA, Darmstadt, Germany) in 160 mL of degassed water, was added slowly under continuous stirring. The temperature was kept constant at 27 °C via a water bath. A black precipitate built up immediately, and the reaction was continued under stable conditions for a further 30 min. Then, the precipitate was washed ~15 times with deionized water via magnetic decantation with a neodymium iron boron magnet in a glass bottle until the conductivity was below 200 $\mu S \text{ cm}^{-1}$. The BIONs were stored under a nitrogen atmosphere at 4 °C. The magnetic susceptibility was analyzed by the SQUID device Quantum Design MPMS XL-7 (Quantum Design GmbH, Darmstadt, Germany). Therefore, the particles were lyophilized, and then they were glued into a small tube. TEM was performed with the JEM 1400 Plus microscope (JEOL GmbH, Freising, Germany), and the recorded images were subsequently evaluated by using ImageJ software.

All experiments were performed either in water ($\eta = 0.888 \text{ mPa s}$, 25 °C) or in a 24% (w/w) sucrose solution ($\eta = 2.227 \text{ mPa s}$, 25 °C, Carl Roth GmbH + Co. KG, Karlsruhe, Germany), fructose solution ($\eta = 1.9858 \text{ mPa s}$, Carl Roth GmbH + Co. KG), or glucose solution ($\eta = 2.1201 \text{ mPa s}$, AppliChem GmbH, Darmstadt, Germany). The pH was

adjusted by adding 0.1 M or 1 M sodium hydroxide (Carl Roth GmbH + Co. KG, Karlsruhe, Germany) or hydrochloric acid (VWR International GmbH, Darmstadt, Germany). A solution of 1 g L⁻¹ BIONs was used, dispersed via an ultrasonication probe (5 min, 10 s on, 15 s off, 20%, Branson Ultrasonics Corporation, Danbury, United States of America). For zeta potential and hydrodynamic diameter by DLS evaluation, a ZetaSizer XS (Malvern Panalytical GmbH, Kassel, Germany) was used. Both measurements were performed at 25 °C in 1 mL of a 1 g L⁻¹ solution in five and three measuring cycles in duplicates, respectively. The IEP was determined by applying a Boltzmann fit.

STEPS were recorded in duplicates at an optical wavelength of 870 nm (LUMiReader, LUM GmbH, Berlin, Germany) to calculate the magnetophoretic velocity. According to Newton's second law of motion, magnetophoresis is composed of the gravitational force F_{grav} , the magnetic force F_{mag} and the viscous drag force F_{drag} , pointing in the opposite direction of the former two forces.

$$\frac{m_p du}{dt} = F_{\text{grav}} + F_{\text{mag}} + F_{\text{drag}} \quad (5)$$

Here, m_p and u are the mass and the velocity of the particle, respectively. For simplicity, the inertial term can be neglected [49,52].

$$0 = F_{\text{grav}} + F_{\text{mag}} + F_{\text{drag}} \quad (6)$$

The magnetic force is determined by the magnetic field gradient ∇H , the permeabilities μ_0 and μ_r , the relative permittivity K , and the particle radius r :

$$F_{\text{mag}} = 3 \cdot \mu_0 \cdot \mu_r \cdot K \cdot \nabla H^2 \cdot 2 \cdot \pi \cdot r^3 \quad (7)$$

According to Stokes' law, the movement of a spherical particle in an incompressible fluid can be described as follows, where η corresponds to the fluid viscosity:

$$F_{\text{drag}} = -6 \cdot u \cdot \pi \cdot \eta \cdot r \quad (8)$$

The gravitational force is based on Newton's law of gravitation,

$$F_{\text{grav}} = \frac{4}{3} (\rho_p - \rho_f) \cdot g \cdot \pi \cdot r^3, \quad (9)$$

which is dependent on the density difference of particle and fluid $\rho_p - \rho_f$ and the free-fall acceleration g . The force balance, as written in Equations (6)–(9), can be solved for the velocity as written in Equation (10):

$$v = \frac{2 \cdot (\rho_p - \rho_f) \cdot g \cdot r^2}{9 \cdot \eta} + \frac{\mu_0 \cdot \mu_r \cdot K \cdot \nabla H^2 \cdot r^2}{2 \cdot \eta} \quad (10)$$

For the measurement, a disposable cuvette (1 × 1 × 4.4 cm) filled with 1 mL of solution was placed onto a stack of five cylindrical neodymium boron ferrite (NdFeB) magnets (diameter = 12 mm, height = 2 mm, N45, Webcraft GmbH, Gottmadingen, Germany). The built-in temperature control assured a constant temperature of 25 °C. The magnetic flux density was measured with a Hall detector PCE-MF M 3000 (PCE Instruments UK Limited, Southampton Hampshire, United Kingdom). The obtained transmittance profiles were integrated over the sample height, leading to an integral transmittance for each measurement time. For data evaluation, it was converted into an integral extinction value, which is directly proportional to the particle concentration after Lambert–Beer's law. Particle movement due to the magnetic and gravitational force induces the change in particle concentration. Therefore, the time-dependent variation of the extinction enables

calculating the magnetophoretic velocity v_{mag} , where L is the mean length defined by half of the sample height.

$$v = \frac{\langle L \rangle}{t} \quad (11)$$

A cumulative distribution function $\Phi(v_{\text{mag}})$ is obtained by plotting the relative extinction over the magnetophoretic velocity [53]. The relative extinction E_{rel} is determined by the initial extinction of the sample E_0 and the minimal extinction E_{min} at the end of magnetophoresis measurement.

$$E_{\text{rel}}(t) = \frac{E - E_{\text{min}}}{E_0 - E_{\text{min}}}, \quad (12)$$

For better comparability, the value at $t_{0.5}$ was used, which is the distribution function's median. It describes the velocity of 50% of the particles at the time $t_{0.5}$, where the extinction has fallen by half. The sedimentation analysis experiments were performed with a magnetic flux density between 40 and 350 mT, which corresponds to a magnetization between 29.31 and 54.40 Am² kg⁻¹.

4. Conclusions

BIONs with an average diameter of 9.2 nm were synthesized via coprecipitation, showing a high saturation magnetization [38]. Zeta potential and hydrodynamic diameter measurements showed that pH and viscosity influence the colloidal stability of the particles. pH values close to the IEP resulted in large particle agglomerates; however, electrostatic stabilization was observed for high and low pH values. The particle distribution over different pHs narrowed due to the increase in viscosity with sucrose. This could be explained by the hydration repulsion and the steric stabilization effect of sucrose. The aggregate size and viscosity directly influence a magnetophoretic process. The particle diameter is proportional to the magnetophoretic velocity, which results in high velocities for large aggregates and lower velocities for small particle diameters. By increasing the viscosity, the drag force counteracts the magnetophoretic force and decreases the magnetophoretic velocity of all aggregate sizes. This study emphasizes the underestimated effect of viscosity by using the simple method of sedimentation analysis, in addition to zeta potential and DLS measurement. In downstream processing or medical applications, liquids such as cell suspension or blood will affect particle migration, resulting in a lower separation. Particularly, the stabilizing effect of sucrose should be further examined, as the formation of aggregates is one of the main reasons for using different coatings for the steric stabilization of the BIONs [54]. In further studies, these new findings can be used to control the aggregation behavior for applications in medicine or biotechnology.

Supplementary Materials: The following are available online at <https://www.mdpi.com/article/10.3390/magnechemistry7060080/s1>, Figure S1: Polydispersity Index of BION suspension from pH 2 to 10 in deionized water ($\eta = 0.888$ mPa s) and sucrose solution ($\eta = 2.227$ mPa s), Figure S2: Intensity distribution data of pH 2 to 10 for high viscous BION suspension. Technical triplicates are shown for each duplicate, Figure S3: Intensity distribution data of pH 2 to 10 for low viscous BION suspension. Technical triplicates are shown for each duplicate, Figure S4: Number distribution of BIONs in fructose, glucose, and sucrose solution at pH 7.

Author Contributions: Conceptualization, L.W. and S.P.S.; methodology, L.W. and C.T.; software, L.W.; validation, L.W.; formal analysis, L.W., C.T.; investigation, L.W.; resources, S.P.S.; data curation, L.W.; writing—original draft preparation, L.W.; writing—review and editing, L.W. and S.P.S.; visualization, L.W.; supervision, S.P.S., project administration, S.P.S.; funding acquisition, S.P.S. All authors have read and agreed to the published version of the manuscript.

Funding: This research was funded by the German Research Foundation (DFG) (Project Number: 441672360). We appreciate the support from the German Research Foundation (DFG) and the Technical University of Munich (TUM) in the framework of the Open-Access Publishing Program and the support by TUM International Graduate School of Science and Engineering (IGSSE).

Institutional Review Board Statement: Not applicable.

Informed Consent Statement: Not applicable.

Data Availability Statement: The original data related to this research can be asked any time to the corresponding author's email: l.wittmann@tum.de.

Acknowledgments: We would like to thank Sonja Berensmeier for laboratory resources and valuable discussions. In addition, we acknowledge Matthias Opel for the SQUID measurement and Carsten Peters for support with TEM imaging.

Conflicts of Interest: The authors declare no conflict of interest. The funders had no role in the design of the study; in the collection, analyses, or interpretation of data; in the writing of the manuscript, or in the decision to publish the results.

References

1. Fraga-García, P.; Kubbutat, P.; Brammen, M.; Schwaminger, S.; Berensmeier, S. Bare Iron Oxide Nanoparticles for Magnetic Harvesting of Microalgae: From Interaction Behavior to Process Realization. *Nanomaterials* **2018**, *8*, 292. [[CrossRef](#)]
2. Schnell, F.; Kube, M.; Berensmeier, S.; Schwaminger, S.P. Magnetic Recovery of Cellulase from Cellulose Substrates with Bare Iron Oxide Nanoparticles. *ChemNanoMat* **2019**, *5*, 422–426. [[CrossRef](#)]
3. Zhang, H.; Ding, W.; Li, S.; Ya, S.; Li, F.; Qiu, B. On-chip analysis of magnetically labeled cells with integrated cell sorting and counting techniques. *Talanta* **2020**, *220*, 121351. [[CrossRef](#)]
4. Puddu, M.; Paunescu, D.; Stark, W.J.; Grass, R.N. Magnetically Recoverable, Thermostable, Hydrophobic DNA/Silica Encapsulates and Their Application as Invisible Oil Tags. *ACS Nano* **2014**, *8*, 2677–2685. [[CrossRef](#)]
5. Ling, W.; Wang, M.; Xiong, C.; Xie, D.; Chen, Q.; Chu, X.; Qiu, X.; Li, Y.; Xiao, X. Synthesis, surface modification, and applications of magnetic iron oxide nanoparticles. *J. Mater. Res.* **2019**, *34*, 1828–1844. [[CrossRef](#)]
6. Liu, S.; Yu, B.; Wang, S.; Shen, Y.; Cong, H. Preparation, surface functionalization and application of Fe₃O₄ magnetic nanoparticles. *Adv. Colloid Interface Sci.* **2020**, *281*, 102165. [[CrossRef](#)]
7. Kodama, R. Magnetic nanoparticles. *Magnetochemistry* **2020**, *6*. [[CrossRef](#)]
8. Massart, R. Preparation of aqueous magnetic liquids in alkaline and acidic media. *IEEE Trans. Magn.* **1981**, *17*, 1247–1248. [[CrossRef](#)]
9. Leong, S.S.; Yeap, S.P.; Lim, J. Working principle and application of magnetic separation for biomedical diagnostic at high- and low-field gradients. *Interface Focus* **2016**, *6*, 20160048. [[CrossRef](#)]
10. Lozar, T.; Jesenko, T.; Prevodnik, V.K.; Cemazar, M.; Hosta, V.; Jericevic, A.; Nolde, N.; Kuhar, C.G. Preclinical and Clinical Evaluation of Magnetic-Activated Cell Separation Technology for CTC Isolation in Breast Cancer. *Front. Oncol.* **2020**, *10*, 1–10. [[CrossRef](#)]
11. Miltenyi, S.; Müller, W.; Weichel, W.; Radbruch, A. High gradient magnetic cell separation with MACS. *Cytometry* **1990**, *11*, 231–238. [[CrossRef](#)]
12. Fratzl, M.; Delshadi, S.; Devillers, T.; Bruckert, F.; Cugat, O.; Dempsey, N.M.; Blaire, G. Magnetophoretic induced convective capture of highly diffusive superparamagnetic nanoparticles. *Soft Matter* **2018**, *14*, 2671–2681. [[CrossRef](#)]
13. Corchero, J.L.; Villaverde, A. Biomedical applications of distally controlled magnetic nanoparticles. *Trends Biotechnol.* **2009**, *27*, 468–476. [[CrossRef](#)] [[PubMed](#)]
14. Toh, P.Y.; Yeap, S.P.; Kong, L.P.; Ng, B.W.; Chan, D.J.C.; Ahmad, A.L.; Lim, J.K. Magnetophoretic removal of microalgae from fishpond water: Feasibility of high gradient and low gradient magnetic separation. *Chem. Eng. J.* **2012**, *211–212*, 22–30. [[CrossRef](#)]
15. Alnaimat, F.; Karam, S.; Mathew, B.; Mathew, B. Magnetophoresis and Microfluidics: A Great Union. *IEEE Nanotechnol. Mag.* **2020**, *14*, 24–41. [[CrossRef](#)]
16. Robert, D.; Pamme, N.; Conjeaud, H.; Gazeau, F.; Iles, A.; Wilhelm, C. Cell sorting by endocytotic capacity in a microfluidic magnetophoresis device. *Lab. Chip* **2011**, *11*, 1902–1910. [[CrossRef](#)] [[PubMed](#)]
17. Kievit, F.M.; Zhang, M. Surface Engineering of Iron Oxide Nanoparticles for Targeted Cancer Therapy. *Acc. Chem. Res.* **2011**, *44*, 853–862. [[CrossRef](#)]
18. Socoliuc, V.; Peddis, D.; Petrenko, V.I.; Avdeev, M.V.; Susan-Resiga, D.; Szabó, T.; Turcu, R.; Tombác, E.; Vékás, L. Magnetic Nanoparticle Systems for Nanomedicine—A Materials Science Perspective. *Magnetochemistry* **2020**, *6*, 2. [[CrossRef](#)]
19. Dulińska-Litewka, J.; Łazarczyk, A.; Hałubiec, P.; Szafranski, O.; Karnas, K.; Karewicz, A. Superparamagnetic Iron Oxide Nanoparticles—Current and Prospective Medical Applications. *Materials* **2019**, *12*, 617. [[CrossRef](#)]
20. Ansari, S.A.M.K.; Ficiara, E.; Ruffinatti, F.A.; Stura, I.; Argenziano, M.; Abollino, O.; Cavalli, R.; Guiot, C.; D'Agata, F. Magnetic Iron Oxide Nanoparticles: Synthesis, Characterization and Functionalization for Biomedical Applications in the Central Nervous System. *Materials* **2019**, *12*, 465. [[CrossRef](#)]
21. Vangijzegem, T.; Stanicki, D.; Laurent, S. Magnetic iron oxide nanoparticles for drug delivery: Applications and characteristics. *Expert Opin. Drug Deliv.* **2019**, *16*, 69–78. [[CrossRef](#)]
22. Soetaert, F.; Korangath, P.; Serantes, D.; Fiering, S.; Ivkov, R. Cancer therapy with iron oxide nanoparticles: Agents of thermal and immune therapies. *Adv. Drug Deliv. Rev.* **2020**, *163–164*, 65–83. [[CrossRef](#)] [[PubMed](#)]

23. Belanova, A.A.; Gavalas, N.; Makarenko, Y.M.; Belousova, M.M.; Soldatov, A.V.; Zolotukhin, P.V. Physicochemical Properties of Magnetic Nanoparticles: Implications for Biomedical Applications In Vitro and In Vivo. *Oncol. Res. Treat.* **2018**, *41*, 139–143. [[CrossRef](#)]
24. Nam, J.; Huang, H.; Lim, H.; Lim, C.; Shin, S. Magnetic Separation of Malaria-Infected Red Blood Cells in Various Developmental Stages. *Anal. Chem.* **2013**, *85*, 7316–7323. [[CrossRef](#)] [[PubMed](#)]
25. Pamme, N.; Wilhelm, C. Continuous sorting of magnetic cells via on-chip free-flow magnetophoresis. *Lab. Chip* **2006**, *6*, 974–980. [[CrossRef](#)] [[PubMed](#)]
26. Roth, H.-C.; Prams, A.; Lutz, M.; Ritscher, J.; Raab, M.; Berensmeier, S. A high-gradient magnetic separator for highly viscous process liquors in industrial biotechnology. *Chem. Eng. Technol.* **2016**, *39*, 469–476. [[CrossRef](#)]
27. Mishima, F.; Hayashi, S.; Akiyama, Y.; Nishijima, S. Development of a Superconducting High Gradient Magnetic Separator for a Highly Viscous Fluid. *IEEE Trans. Appl. Supercond.* **2011**, *22*, 3700204. [[CrossRef](#)]
28. Gupta, A.K.; Gupta, M. Synthesis and surface engineering of iron oxide nanoparticles for biomedical applications. *Biomaterials* **2005**, *26*, 3995–4021. [[CrossRef](#)]
29. Coppola, L.; Caserta, F.; De Lucia, D.; Guastafierro, S.; Grassia, A.; Coppola, A.; Marfella, R.; Varricchio, M. Blood viscosity and aging. *Arch. Gerontol. Geriatr.* **2000**, *31*, 35–42. [[CrossRef](#)]
30. Alphandéry, E. Bio-synthesized iron oxide nanoparticles for cancer treatment. *Int. J. Pharm.* **2020**, *586*, 119472. [[CrossRef](#)]
31. Solsona, M.; Nieuwelink, A.-E.; Meirer, F.; Abelmann, L.; Odijk, M.; Olthuis, W.; Weckhuysen, B.M.; Berg, A.V.D. Magnetophoretic Sorting of Single Catalyst Particles. *Angew. Chem. Int. Ed.* **2018**, *57*, 10589–10594. [[CrossRef](#)] [[PubMed](#)]
32. Faraudo, J.; Andreu, J.S.; Calero, C.; Camacho, J. Predicting the Self-Assembly of Superparamagnetic Colloids under Magnetic Fields. *Adv. Funct. Mater.* **2016**, *26*, 3837–3858. [[CrossRef](#)]
33. Leong, S.S.; Ahmad, Z.; Low, S.C.; Camacho, J.; Faraudo, J.; Lim, J. Unified View of Magnetic Nanoparticle Separation under Magnetophoresis. *Langmuir* **2020**, *36*, 8033–8055. [[CrossRef](#)]
34. Yavuz, C.T.; Mayo, J.T.; Yu, W.W.; Prakash, A.; Falkner, J.C.; Yean, S.; Cong, L.; Shipley, H.J.; Kan, A.; Tomson, M.; et al. Low-Field Magnetic Separation of Monodisperse Fe₃O₄ Nanocrystals. *Science* **2006**, *314*, 964–967. [[CrossRef](#)]
35. Faraudo, J.; Camacho, J. Cooperative magnetophoresis of superparamagnetic colloids: Theoretical aspects. *Colloid Polym. Sci.* **2009**, *288*, 207–215. [[CrossRef](#)]
36. Schwaminger, S.P.; Fraga-García, P.; Selbach, F.; Hein, F.G.; Fuß, E.C.; Surya, R.; Roth, H.-C.; Blank-Shim, S.A.; Wagner, F.E.; Heissler, S.; et al. Bio-nano interactions: Cellulase on iron oxide nanoparticle surfaces. *Adsorption* **2016**, *23*, 281–292. [[CrossRef](#)]
37. Bean, C.P.; Livingston, J.D. Superparamagnetism. *J. Appl. Phys.* **1959**, *30*, S120–S129. [[CrossRef](#)]
38. Turrina, C.; Berensmeier, S.; Schwaminger, S. Bare Iron Oxide Nanoparticles as Drug Delivery Carrier for the Short Cationic Peptide Lasioglossin. *Pharmaceuticals* **2021**, *14*, 405. [[CrossRef](#)]
39. Schwaminger, S.; Syhr, C.; Berensmeier, S. Controlled Synthesis of Magnetic Iron Oxide Nanoparticles: Magnetite or Maghemite? *Crystals* **2020**, *10*, 214. [[CrossRef](#)]
40. Schwaminger, S.P.; Bauer, D.; Fraga-García, P.; Wagner, F.E.; Berensmeier, S. Oxidation of magnetite nanoparticles: Impact on surface and crystal properties. *CrystEngComm* **2016**, *19*, 246–255. [[CrossRef](#)]
41. Schwaminger, S.P.; Schwarzenberger, K.; Gatzemeier, J.; Lei, Z.; Eckert, K. Magnetically Induced Aggregation of Iron Oxide Nanoparticles for Carrier Flotation Strategies. *ACS Appl. Mater. Interfaces* **2021**, *13*, 20830–20844. [[CrossRef](#)] [[PubMed](#)]
42. Schwaminger, S.P.; Blank-Shim, S.A.; Scheifele, I.; Fraga-García, P.; Berensmeier, S. Peptide binding to metal oxide nanoparticles. *Faraday Discuss.* **2017**, *204*, 233–250. [[CrossRef](#)] [[PubMed](#)]
43. Stetefeld, J.; McKenna, S.; Patel, T.R. Dynamic light scattering: A practical guide and applications in biomedical sciences. *Biophys. Rev.* **2016**, *8*, 409–427. [[CrossRef](#)] [[PubMed](#)]
44. Szalai, A.J.; Manivannan, N.; Kaptay, G. Super-paramagnetic magnetite nanoparticles obtained by different synthesis and separation methods stabilized by biocompatible coatings. *Colloids Surfaces A Physicochem. Eng. Asp.* **2019**, *568*, 113–122. [[CrossRef](#)]
45. Sun, X.; Zheng, C.; Zhang, F.; Yang, Y.; Wu, G.; Yu, A.; Guan, N. Size-Controlled Synthesis of Magnetite (Fe₃O₄) Nanoparticles Coated with Glucose and Gluconic Acid from a Single Fe(III) Precursor by a Sucrose Bifunctional Hydrothermal Method. *J. Phys. Chem. C* **2009**, *113*, 16002–16008. [[CrossRef](#)]
46. Cushing, B.L.; Kolesnichenko, V.; O'Connor, C.J. Recent Advances in the Liquid-Phase Syntheses of Inorganic Nanoparticles. *Chem. Rev.* **2004**, *104*, 3893–3946. [[CrossRef](#)] [[PubMed](#)]
47. Benítez, E.I.; Genovese, D.B.; Lozano, J.E. Effect of typical sugars on the viscosity and colloidal stability of apple juice. *Food Hydrocoll.* **2009**, *23*, 519–525. [[CrossRef](#)]
48. Chalikian, T.V. Ultrasonic and Densimetric Characterizations of the Hydration Properties of Polar Groups in Monosaccharides. *J. Phys. Chem. B* **1998**, *102*, 6921–6926. [[CrossRef](#)]
49. Leong, S.S.; Ahmad, Z.; Lim, J. Magnetophoresis of superparamagnetic nanoparticles at low field gradient: Hydrodynamic effect. *Soft Matter* **2015**, *11*, 6968–6980. [[CrossRef](#)]
50. Cuevas, G.D.L.; Faraudo, J.; Camacho, J. Low-Gradient Magnetophoresis through Field-Induced Reversible Aggregation. *J. Phys. Chem. C* **2008**, *112*, 945–950. [[CrossRef](#)]
51. Einstein, A. Über die von der molekularkinetischen Theorie der Wärme geforderte Bewegung von in ruhenden Flüssigkeiten suspendierten Teilchen. *Ann. Phys.* **1905**, *322*, 549–560. [[CrossRef](#)]
52. Furlani, E.P. Analysis of particle transport in a magnetophoretic microsystem. *J. Appl. Phys.* **2006**, *99*, 024912. [[CrossRef](#)]

-
53. Mykhaylyk, O.; Lerche, D.; Vlaskou, D.; Schoemig, V.; Detloff, T.; Krause, D.; Wolff, M.; Joas, T.; Berensmeier, S.; Plank, C.; et al. Biomagnetic Particles Magnetophoretic Velocity Determined by Space- and Time-Resolved Extinction Profiles. *IEEE Magn. Lett.* **2015**, *6*, 1–4. [[CrossRef](#)]
 54. Laurent, S.; Forge, D.; Port, M.; Roch, A.; Robic, C.; Elst, L.V.; Muller, R.N. Erratum: Magnetic Iron Oxide Nanoparticles: Synthesis, Stabilization, Vectorization, Physicochemical Characterizations, and Biological Applications. *Chem. Rev.* **2008**, *110*, 2574. [[CrossRef](#)]